Dalton Transactions

RSC Publishing

COMMUNICATION

View Article Online
View Journal | View Issue

Cite this: *Dalton Trans.*, 2013, **42**, 7529

Received 8th February 2013,
Accepted 4th April 2013

DOI: 10.1039/c3dt50887k

www.rsc.org/dalton

Highly soluble iron- and nickel-substituted decaniobates with tetramethylammonium countercations†

Jung-Ho Son,[a] C. André Ohlin[b] and William H. Casey*[a]

Iron- and nickel-substituted decaniobates, $[H_2Fe^{III}Nb_9O_{28}]^{6-}$ and $[H_3Ni^{II}Nb_9O^{28}]^{6-}$ were hydrothermally synthesized as tetramethylammonium salts and the structures were determined by X-ray crystallography. The highly soluble title compounds were characterized by ESI-MS, FT-IR and UV-Vis titration.

Polyoxometalates are a unique class of molecular ions which find importance in fields such as catalysis, medicine and materials science.[1] Many kinds of tungsten-, molybdenum- and vanadium-based polyoxometalates are known, and their large structural diversity arises from the inclusion of heteroatoms.[2] In contrast, only a small number of substituted polyoxoniobates have been isolated, partly because $[Nb_{10}O_{28}]^{6-}$ (decaniobate, Nb_{10}) and $[Nb_6O_{19}]^{8-}$ (hexaniobate) ions dominate under their hydrothermal synthesis conditions.[3] A limited number of main-group element substituted polyoxoniobates has been synthesized during mainly the last decade.[4] In particular, few examples of transition metal substituted polyoxoniobate ions have been reported so far, with Ti^{IV}-substituted polyoxoniobates including $[Ti_2Nb_8O_{28}]^{8-}$, $[TiNb_9O_{28}]^{7-}$, and $[Ti_{12}Nb_6O_{44}]^{10-}$.[5] More recently vanadium-substituted niobates such as $[VNb_{12}O_{40}(VO)_2]^{9-}$, $[Nb_{10}V_4O_{40}(OH)_2]^{12-}$, and $[H_6V_4Nb_6O_{30}]^{4-}$ have been characterized.[6] In addition, copper- and chromium-substituted polyoxoniobates such as $[CuNb_{11}O_{35}H_4]^{9-}$ and $[Cr_2(OH)_4Nb_{10}O_{30}]^{8-}$ were also reported.[7]

Iron and nickel containing polyoxotungstates and -molybdates have been extensively studied for their catalytic, electrochemical, and magnetic properties.[8] Analogously, polyoxoniobates containing iron or nickel would be of interest in many fields, but they are not known to date due to the synthetic challenges. Herein we report the first synthesis and characterization of iron- and nickel-substituted decaniobates as soluble tetramethylammonium (TMA) salts; $TMA_6[H_2Fe^{III}Nb_9O_{28}]\cdot 14H_2O$ (**1**) and $TMA_6[H_3Ni^{II}Nb_9O_{28}]\cdot 17H_2O$ (**2**).

The syntheses were carried out by hydrothermal reaction of a mixture of niobic acid (hydrous niobium oxide), TMAOH and a metal salt; K_2FeO_4 or $FeCl_3\cdot 6H_2O$ for **1** and $NiCl_2\cdot 6H_2O$ for **2** were used. The same cluster $[H_2Fe^{III}Nb_9O_{28}]^{6-}$ formed regardless of whether we chose K_2FeO_4 or $FeCl_3\cdot 6H_2O$ as an iron source, as confirmed by X-ray crystallography and electrospray-ionization mass spectrometry (ESI-MS), suggesting that the Fe^{VI} in K_2FeO_4 was reduced. This is understandable since K_2FeO_4 is a strong oxidizing agent and the reaction was carried out under hydrothermal conditions under which the TMA cation can undergo thermal decomposition and cause reduction. It was important to optimize the reaction conditions due to the concurrent formation of decaniobate or hexaniobate, which hampered purification and resulted in the easy formation of co-crystals of decaniobate and transition metal-substituted decaniobate due to their nearly identical shapes and charges.

The identity of Fe^{III}- and Ni^{II}-substituted decaniobates was confirmed by using ESI-MS (Fig. 1). The ESI-MS spectra of **1** and **2** are similar but distinguishable, having slightly different peak positions due to the similar masses of ^{56}Fe (55.935 amu; 92% abundance) and ^{58}Ni (57.935 amu; 68% abundance), and the peaks are at lower m/z values than the corresponding peaks of the TMA salt of Nb_{10},[9] due to the substitution of lighter, early transition metals in place of niobium (Fig. 1). Ions with a charge of −2 were found in the 400 and 500 m/z range, and $z = -3$ ions appeared in the 700–800 m/z range. Both Ni and Fe have several naturally occurring isotopes, and the isotopic fingerprint confirmed the inclusion of the corresponding transition metal in the cluster (Fig. S1,† ESI).

The crystal structures indicate that the substitution occurs at the central metal site of the decaniobate ion, which is the only site without a terminal oxygen group. In the crystal structure of **1**‡, the iron atom is disordered among the two central

[a]*Department of Chemistry, University of California, Davis, One Shields Ave, Davis, CA 95616, USA. E-mail: whcasey@ucdavis.edu; Fax: (+1) (530) 752 8995*
[b]*School of Chemistry, Monash University, Clayton, Victoria 3800, Australia*

†Electronic supplementary information (ESI) available: Synthetic procedure, X-ray single crystal structure refinement parameter, simulated ESI-MS, ESI-MS after base titration, UV-Vis titration, potentiometric titration data, and TD-DFT simulation result of UV-Vis spectra of **1** and **2**. CCDC 919660 and 919661. For ESI and crystallographic data in CIF or other electronic format see DOI: 10.1039/c3dt50887k

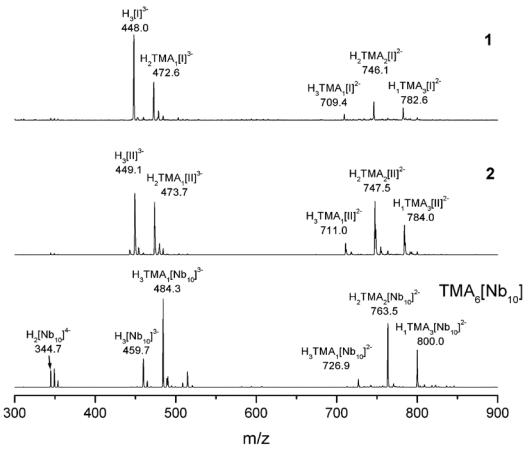

Fig. 1 ESI-MS of **1**, **2** and TMA salt of $[Nb_{10}O_{28}]^{6-}$. [I] = $[H_2Fe^{III}Nb_9O_{28}]$, [II] = $[H_3Ni^{II}Nb_9O_{28}]$, $[Nb_{10}]$ = $[Nb_{10}O_{28}]$.

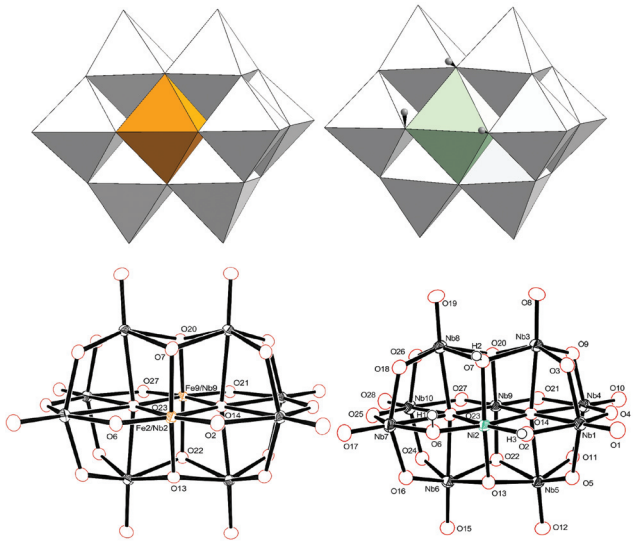

Fig. 2 The structures of $[H_2Fe^{III}Nb_9O_{28}]^{6-}$ (left) and $[H_3Ni^{II}Nb_9O_{28}]^{6-}$ (right) in **1** and **2**, respectively, drawn with polyhedral (top, Nb: white, Fe: orange, Ni: green and H: gray) and thermal ellipsoid model (bottom). Thermal ellipsoids are drawn at 50% probability level.

sites due to the symmetry of the molecule (Fig. 2). Structure refinement with a partial occupancy model indicates that the iron occupancies in the Fe2/Nb2 and Fe9/Nb9 sites are 0.7 and 0.3, respectively. Thus the stoichiometry of metals in the cluster is one iron and nine niobium atoms, which agrees with the ESI-MS data. The Fe2 site shows different M–O lengths due to the higher iron character, *e.g.* longer Fe–μ_2-O lengths (1.908(2) and 1.922(2) Å) and shorter Fe–μ_6-O lengths (2.131(2) and 2.154(2) Å), compared to the corresponding Nb–O lengths in Nb_{10} with Nb–μ_2-O of 1.8365(26) and 1.8373(19) Å, and Nb–μ_6-O of 2.2109(25) and 2.2307(18) Å. Overall, the central Fe–O octahedron in $FeNb_9O_{28}$ is more symmetric than that in Nb_{10} (Table 1). The Fe9 site, where 0.3 parts of iron is located, has only slightly longer Fe–μ_2-O lengths (1.860(2) and 1.863(2) Å) and shorter Fe–μ_6-O lengths (2.187(2) and 2.208(2) Å)

Table 1 Comparison of M–O bond lengths at the central sites in decaniobate,[9] Ti-substituted decaniobate[5c] with **1** and **2**. Numbers indicate bond lengths in Å

Bond	$[Nb_{10}O_{28}]^{6-}$	$[TiNb_9O_{28}]^{7-}$	$[H_2FeNb_9O_{28}]^{6-}$	$[H_3NiNb_9O_{28}]^{6-}$
M–μ_2-O	1.8365(26) 1.8373(19)	1.8138(42) 1.8241(42)	1.9078(21) 1.9221(25)	1.9827(33) 2.0194(34)
M–μ_3-O	2.0055(19) 2.0248(20)	2.0029(30) 2.0192(31)	2.0016(24) 2.0748(23)	2.0996(25) 2.1841(24)
M–μ_6-O	2.2109(25) 2.2307(18)	2.1825(44) 2.2086(43)	2.1307(24) 2.1544(22)	2.1242(31) 2.1246(30)

compared to those in Nb_{10} because of the smaller iron portion in this site than Fe2 site. The bond valence sum (BVS) calculation[10] indicates that the iron has an oxidation state of +3 (2.969 for Fe2 and 3.095 for Fe9). This calculation suggests that the cluster should carry a charge of −8 with a stoichiometry of $[Fe^{III}Nb_9O_{28}]^{8-}$. However, only 6 TMA counter-cations are found in the crystal structure, suggesting the cluster ion is probably protonated. Although no protons were found in the electron density map because of disorder, BVS calculations of the oxygen atoms indicate that the two bridging μ_2 oxygen atoms between the Fe2 and equatorial Nb sites are protonated. BVS calculation of the bridging oxygen atoms shows that the two μ_2-O bonded to Fe2 are most probable sites for protonation (1.212 for O2 and for 1.271 for O6) as their values are significantly smaller than the corresponding BVS values for the other structural oxygen atoms which are closer to 2. Similarly, the two μ_2-O bonded to Fe9 are also partly protonated, with bond valence sums of 1.352 and 1.361 for O21 and O27, respectively. Thus the empirical formula of the cluster is expressed as $[H_2Fe^{III}Nb_9O_{28}]^{6-}$.

In the crystal structure of the nickel-substituted decaniobate **2**, the nickel site is not disordered in the two central metal sites as was the case in **1**, thus allowing for clearer M–O length comparisons of the substituted site than in **1** (Fig. 2). The Ni–μ_2-O bonds (1.983(3) and 2.019(3) Å) in **2** are even much longer than the Fe–μ_2-O bonds in **1**. The Ni–μ_6-O lengths (2.124(3) Å) are slightly shorter than the Fe–μ_6-O bond lengths in **1**. It is noted that Ni–μ_3-O bond lengths (2.100(3) and 2.184(3) Å) in **2** are asymmetric and significantly longer than corresponding bonds in both **1** and Nb_{10} (Table 1). In nickel-substituted decaniobate, three hydrogen atoms were found on the cluster from the electron density map during the final crystal structure refinements. Two protons are located on the two μ_2-O (O2 and O6) between Ni and Nb, and another proton is found on one of the μ_3-O (O7), which has longer Ni–μ_3-O length (2.184(3) Å) than the other μ_3-O in the *trans* position (O13, 2.100(3) Å). In addition, O7 has much longer Nb–O lengths (2.175(3) and 2.200(3) Å) than O13 (2.016(3) and 2.017(3) Å), supporting the protonation of O7. The BVS calculations of O2 (1.158), O6 (1.033) and O7 (1.201) agree with the suggested protonation configuration, which is much closer to unity than that of the unprotonated oxygen site O13 (1.821). The BVS calculation indicates an oxidation state of Ni^{II} (1.994).

The cluster as it is found in the solid state, $[H_3Ni^{II}Nb_9O_{28}]^{6-}$, has the same −6 charge as $[Nb_{10}O_{28}]^{6-}$ and $[H_2Fe^{III}Nb_9O_{28}]^{6-}$, and we found about six charge-compensating TMA countercations; among these, one TMA is highly disordered in two different locations with nearby crystallization water molecules.

In solid-state structure, **1** and **2** have different packing motifs. The clusters $[H_2Fe^{III}Nb_9O_{28}]^{6-}$ are fairly isolated from each other in the crystal structure of **1** with closest Fe···Fe distance of 10.1 Å, while the $[H_3Ni^{II}Nb_9O_{28}]^{6-}$ clusters form hydrogen-bonded dimers in **2** with Ni···Ni distance of 6.1 Å. Six hydrogen bonds are found in the dimeric assembly (Fig. S2,† ESI). The $[H_3Ni^{II}Nb_9O_{28}]^{6-}$ clusters form hydrogen bonds to each other *via* their surface protons, as has been previously demonstrated from the analogously Pt-substituted decavanadate, $[H_2PtV_9O_{28}]^{5-}$.[11] We also note that substituted decavanadates such as $[H_2MoV_9O_{28}]^{3-}$, $[HTeV_9O_{28}]^{4-}$ and $[IV_9O_{28}]^{4-}$ have been reported, but these clusters do not form hydrogen-bonded dimers in their solid-state structure.[12] Correlated with the solid-state structures, we have observed slightly different solubility of **1** and **2**. Both **1** and **2** are very soluble in water, soluble in methanol. In ethanol, however, **1** is moderately soluble but **2** is poorly soluble, which we attribute to the different solid-state packings. This might be because hydrogen-bonded dimeric clusters in **2** are more difficult to be solvated in ethanol than the isolated clusters in **1**.

The solubility of the compounds in water is on the order of a gram per milliliter. The compounds are also soluble in methanol (1 g mL^{-1} for **1** and 0.13 g mL^{-1} for **2**) and sparingly soluble in ethanol (4 mg mL^{-1} for **1** and 1 mg mL^{-1} for **2**). There are several advantages associated with increased solubility since it makes it possible to dissolve enough compounds for analysis, as well as chemistry. In particular, applications that involve deposition or homogeneous photo- or electrochemistry benefit from improved solubility.

FT-IR spectra of **1** and **2** show similar features but differ from the spectrum of the TMA salt of Nb_{10} (Fig. 3), probably owing to the lower symmetries in the monosubstituted decametalate structures. The IR spectrum of TMA salt of Nb_{10} matches well with the reported spectra of TMA or tetrabutylammonium salt of Nb_{10}.[13] In the spectra of **1** and **2**, the stretching bands of Nb=O_t bond appear near 955 and 900 cm^{-1}, partly overlapped with the band of TMA ion. The bands near 800 and 740 cm^{-1} are assigned as Nb–O asymmetric stretching modes. A weaker band at 675 cm^{-1} in the spectra of **1** and **2** could be from ν_{as}(M–OH) stretching, based on the band assignment from the protonated decavanadate, where the ν_{as}(V–OH) vibration appeared at 630 cm^{-1}.[14] Three symmetric stretching Nb–O bands at 584, 534, and 502 cm^{-1} in Nb_{10} are indistinguishable in the spectra of **1** and **2** by showing single broad band centered at 527 and 533 cm^{-1}, respectively. The Nb–O bending mode appears near 430 cm^{-1}.

UV-Vis spectra of **1** and **2** were collected during the titration with either TMAOH or HCl solution to check the acid–base behavior of the substituted niobate clusters (Fig. 4, Fig. S4–6,† ESI). The initial pH values of 5 mM solutions of **1** and **2** with 0.1 M TMACl as a background salt were 7.9 and 7.5, respectively, and these solutions were used as the starting solutions for UV-Vis titration experiments. These higher concentration solutions were necessary to observe the change in the visible region by the incorporation of the Fe or Ni, since the compounds are very weakly absorbing in the visible region, consistent with the fact that only one tenth of the metal sites are colour-inducing atoms in **1** and **2**. The UV-Vis spectrum of **1** shows an absorption from Fe^{III} at *ca.* 480 nm from the $2(^6A_1) \rightarrow 2(^4T_1)$ transition in 5 mM solution.[15] The UV-Vis spectrum of **2** shows two characteristic absorptions at 410 and 700 nm from the hexa-coordinate oxo Ni^{II} in the cluster which are from $^3A_{2g} \rightarrow {}^3T_{1g}(P)$ and $^3A_{2g} \rightarrow {}^3T_{1g}(F)$ transitions, respectively.[16] Neither of the UV-Vis spectra of **1** and **2** changed

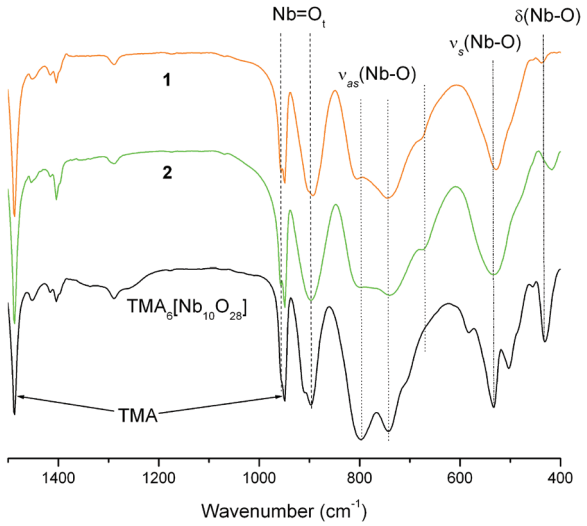

Fig. 3 FT-IR spectra of **1** (orange), **2** (green) and TMA salt of $[Nb_{10}O_{28}]^{6-}$ (black).

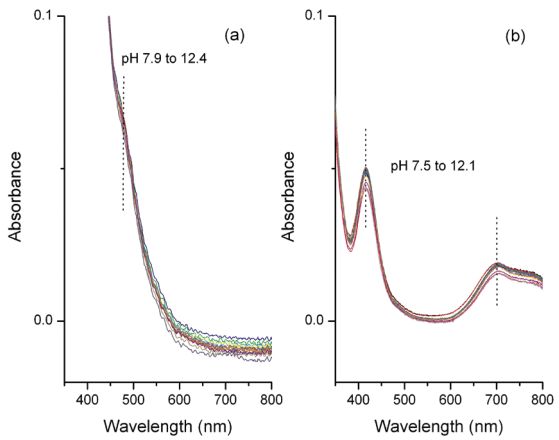

Fig. 4 Overlain UV-Vis spectra of (a) **1** (15 spectra) and (b) **2** (18 spectra) during the titration with TMAOH solution. The spectra show little changes in these pH ranges (sample concentration 5 mM in 0.1 M TMACl as a background salt).

significantly until *ca.* pH 12 when titrating with TMAOH, indicating that the clusters are stable under moderately strong basic conditions (Fig. 4). The ESI-MS spectra of the solution after the titration experiment after months showed peaks corresponding to **1** and **2** as the main components of the spectra with a relatively much smaller abundance of hexaniobate peaks, which may have formed due to the strongly basic conditions during the titration (Fig. S3,† ESI). Thus both UV-Vis and ESI-MS data indicate that **1** and **2** are stable in basic solutions.

When titrating the 5 mM solutions of **1** and **2** from their natural pH in the acidic direction, precipitate formed immediately upon each addition of dilute HCl before mixing. The colloids are apparently polydisperse, and settle out from solution over several hours. The formation of hydrous niobium oxide in acidic condition is a common phenomenon, which is reported in the preceding literatures.[17] We interpret the cause as irreversible proton-induced condensation as each drop of HCl solution mixed into solution; these colloids causes an increase in absorbance over the entire spectral range (Fig. S4,† ESI). Thus determining the stability in the acidic condition was not possible using 5 mM solutions. When more dilute 0.027 mM solutions were titrated with HCl, the absorbance in the UV range started to increase below pH 4.8 for **1** and pH 5.1 for **2**, indicating the condensation into colloids at low pH (Fig. S5,† ESI). The Tyndall effect was observed at these low pH conditions and both solutions of **1** and **2** conspicuously formed precipitate below pH 4, where the overall absorption started to decrease. During the titration of the 0.027 mM solutions of **1** and **2** with TMAOH, the LMCT bands in the UV region at 240 nm and 310 nm in **1** and 230 nm in **2** only slightly increased until pH 12.5, supporting the stability in the basic region as determined from the UV-Vis titration results of the 5 mM solutions (Fig. S6,† ESI).

Overall, the UV-Vis titration data showed only monotonous changes, suggesting either that deprotonation of the cluster is not occurring even in the highly basic condition (Fig. S7,† ESI) or that deprotonation was not associated with changes in absorbance. Increased absorbance at 200 nm in strong basic condition is due to increased concentration of TMAOH. No pK_a value could be confidently assigned from the potentiometric titration curve (Fig. S8,† ESI) or from the UV-Vis data, although attempts were made using nonlinear regression analysis.

In summary, we report the isolation and characterization of the unprecedented iron- and nickel-substituted polyoxoniobates as highly soluble TMA salt, with the new clusters being stable between 6 < pH < 12. These new compounds will be of interest in their catalytic, electrochemical, magnetic and photochemical studies due to their inclusion of single transition metal site in the decaniobate framework. The fact that both divalent and trivalent metals can be substituted into the decaniobate framework extends our attempts to understand the relation between overall molecular charge in this decametalate structural class and reactivity to oxygen-isotope exchanges.

Acknowledgements

This work was supported by an NSF CCI grant through the Center for Sustainable Materials Chemistry, number CHE-1102637. CAO is grateful for a Queen Elizabeth II (QEII) fellowship and a Discovery Project grant (DP110105530) awarded by the Australian Research Council.

Notes and references

‡*Crystal data.* (**1**) CCDC 919660: $C_{24}H_{87}N_6FeNb_9O_{42.12}$, M = 2029.04, monoclinic, a = 16.6125(14), b = 17.2040(14), c = 24.080(2) Å, β = 105.990(1)°, U = 6615.9(10) Å^3, T = 90 K, space group $P2_1/n$ (no. 14), Z = 4, 71 533 reflections measured, 15 188 unique (R_{int} = 0.0348) which were used in all calculations. The final w$R(F^2)$ was 0.0754 (all data). (**2**) CCDC 919661. $C_{24.16}H_{69.76}N_{6.14}NiNb_9O_{44.96}$, M = 2057.76, triclinic, a = 12.9120(11), b = 16.1127(14), c = 18.4177(16) Å, α = 75.726(1), β = 74.247(1), γ = 69.871(1)°, U = 3412.5(5) Å^3, T = 90 K, space group $P\bar{1}$ (no. 2), Z = 2, 37 319 reflections measured, 15 419 unique (R_{int} = 0.0171) which were used in all calculations. The final w$R(F^2)$ was 0.0894 (all data).

1 (*a*) M. T. Pope, *Heteropoly and Isopolyoxometalates*, Springer-Verlag, Berlin, 1983; (*b*) M. T. Pope and A. Müller, *Angew. Chem., Int. Ed. Engl.*, 1991, **30**, 34–48; (*c*) *Polyoxometalates. From Platonic Solids to Anti-Retroviral Activity*, ed. M. T. Pope and A. Müller, Kluwer Academic Publishers, Dordrecht, The Netherlands, 1994; (*d*) C. L. Hill, ed. Special volume on "*Polyoxometalates*", *Chem. Rev.*, 1998, **98**, 1–390; (*e*) C. Ritchie, A. Ferguson, H. Nojiri, H. N. Miras, Y.-F. Song, D.-L. Long, E. Burkholder, M. Murrie, P. Kögerler, E. K. Brechin and L. Cronin, *Angew. Chem., Int. Ed.*, 2008, **47**, 5609–5612; (*f*) J.-D. Compain, P. Mialane, A. Dolbecq, I. Mbomekallé, J. Marrot, F. Sécheresse, E. Rivière, G. Rogez and W. Wernsdorfer, *Angew. Chem.*, 2009, **121**, 3123–3127.

2 (*a*) *Polyoxometalate Molecular Science*, ed. J. J. Borrás-Almenar, E. Coronado, A. Müller and M. T. Pope, Springer, 2003; (*b*) U. Kortz, A. Müller, J. van Slageren, J. Schnack, N. S. Dalal and M. Dressel, *Coord. Chem. Rev.*, 2009, **253**, 2315–2327; (*c*) D.-L. Long, R. Tsunashima and L. Cronin, *Angew. Chem., Int. Ed.*, 2010, **49**, 1736–1758; (*d*) S.-T. Zheng and G.-Y. Yang, *Chem. Soc. Rev.*, 2012, **41**, 7623–7646.

3 M. Nyman, *Dalton Trans.*, 2011, **40**, 8049–8058.

4 (*a*) M. Nyman, F. Bonhomme, T. M. Alam, M. A. Rodriguez, B. R. Cherry, J. L. Krumhansl, T. M. Nenoff and A. M. Sattler, *Science*, 2002, **297**, 996–998; (*b*) M. Nyman, F. Bonhomme, T. M. Alam, J. B. Parise and G. M. B. Vaughan, *Angew. Chem., Int. Ed.*, 2004, **43**, 2787–2792; (*c*) T. M. Anderson, S. G. Thoma, F. Bonhomme, M. A. Rodriguez, H. Park, J. B. Parise, T. M. Alam, J. P. Larentzos and M. Nyman, *Cryst. Growth Des.*, 2007, **7**, 719–723; (*d*) F. Bonhomme, J. P. Larentzos, T. M. Alam, E. J. Maginn and M. Nyman, *Inorg. Chem.*, 2005, **44**, 1774–1785; (*e*) M. Nyman, A. J. Celestian, J. B. Parise, G. P. Holland and T. M. Alam, *Inorg. Chem.*, 2006, **45**, 1043–1052; (*f*) M. Nyman, J. P. Larentzos, E. J. Maginn, M. E. Welk, D. Ingersoll, H. Park, J. B. Parise, I. Bull and F. Bonhomme, *Inorg. Chem.*, 2007, **46**, 2067–2079;

(*g*) Y. Hou, M. Nyman and M. Rodriguez, *Angew. Chem., Int. Ed.*, 2011, **50**, 12514–12517.

5 (*a*) M. Nyman, L. J. Criscenti, F. Bonhomme, M. A. Rodriguez and R. T. Cygan, *J. Solid State Chem.*, 2003, **176**, 111–119; (*b*) C. A. Ohlin, E. M. Villa, J. C. Fettinger and W. H. Casey, *Angew. Chem., Int. Ed.*, 2008, **47**, 5634–5636; (*c*) C. A. Ohlin, E. M. Villa, J. C. Fettinger and W. H. Casey, *Dalton Trans.*, 2009, 2677–2678.

6 (*a*) G. Guo, Y. Xu, J. Cao and C. Hu, *Chem. Commun.*, 2011, **47**, 9411–9413; (*b*) G. Guo, Y. Xu, J. Cao and C. Hu, *Chem.–Eur. J.*, 2012, **18**, 3493–3497; (*c*) P. Huang, C. Qin, X.-L. Wang, C.-Y. Sun, G.-S. Yang, K.-Z. Shao, Y.-Q. Jiao, K. Zhou and Z.-M. Su, *Chem. Commun.*, 2012, **48**, 103–105; (*d*) J.-H. Son, C. A. Ohlin, E. C. Larson, P. Yu and W. H. Casey, *Eur. J. Inorg. Chem.*, 2013, 1748–1753.

7 (*a*) J.-Y. Niu, G. Chen, J.-W. Zhao, P.-T. Ma, S.-Z. Li, J.-P. Wang, M.-X. Li, Y. Bai and B.-S. Ji, *Chem.–Eur. J.*, 2010, **16**, 7082–7086; (*b*) J.-H. Son, C. A. Ohlin and W. H. Casey, *Dalton Trans.*, 2012, **41**, 12674–12677.

8 (*a*) X. Zhang, Q. Chen, D. C. Duncan, R. J. Lachicotte and C. L. Hill, *Inorg. Chem.*, 1997, **36**, 4381–4386; (*b*) U. Kortz, Y. P. Jeannin, A. Teze, G. Herve and S. Isber, *Inorg. Chem.*, 1999, **38**, 3670–3675; (*c*) J. M. Clemente-Juan and E. Coronado, *Coord. Chem. Rev.*, 1999, **193**, 361–394; (*d*) R. Ben-Daniel, A. M. Khenkin and R. Neumann, *Chem.–Eur. J.*, 2000, **6**, 3722–3728; (*e*) J. E. Toth and F. C. Anson, *J. Am. Chem. Soc.*, 1989, **111**, 2444–2451; (*f*) R. Contant, M. Abbessi, J. Canny, A. Belhouari, B. Keita and L. Nadjo, *Inorg. Chem.*, 1997, **36**, 4961–4967; (*g*) U. Kortz, I. M. Mbomekalle, B. Keita, L. Nadjo and P. Berthet, *Inorg. Chem.*, 2002, **41**, 6412–6416.

9 C. A. Ohlin, E. M. Villa and W. H. Casey, *Inorg. Chim. Acta*, 2009, **362**, 1391–1392.

10 I. D. Brown and D. Altermatt, *Acta Crystallogr., Sect. B: Struct. Sci.*, 1985, **41**, 244–247.

11 U. Lee, H.-C. Joo, K.-M. Park, S. S. Mal, U. Kortz, B. Keita and L. Nadjo, *Angew. Chem., Int. Ed.*, 2008, **47**, 793–796.

12 (*a*) N. Strukan, M. Cindrić and B. Kamenar, *Polyhedron*, 1997, **16**, 629–634; (*b*) S. Konaka, Y. Ozawa and A. Yagasaki, *Inorg. Chem. Commun.*, 2008, **11**, 1267–1269; (*c*) S. Konaka, Y. Ozawa, T. Shonaka, S. Watanabe and A. Yagasaki, *Inorg. Chem.*, 2011, **50**, 6183–6188; (*d*) A. Fukui, Y. Ozawa and A. Yagasaki, *Polyhedron*, 2012, **42**, 149–152.

13 (*a*) M. Matsumoto, Y. Ozawa and A. Yagasaki, *Polyhedron*, 2010, **29**, 2196–2201; (*b*) W. G. Klemperer and K. A. Marek, *Eur. J. Inorg. Chem.*, 2013, 1762–1771.

14 P. Román, A. Aranzabe, A. Luque, J. M. Gutiérrez-Zorrilla and M. Martínez-Ripoll, *J. Chem. Soc., Dalton Trans.*, 1995, 2225–2231.

15 R. M. Cornell and U. Schwertmann, *The Iron Oxides*, John Wiley & Sons, 2006.

16 F. A. Cotton, G. Wilkinson, C. A. Murillo and M. Bochmann, *Advanced Inorganic Chemistry*, Wiley-Interscience, New York, 6th edn, 1999.

17 (*a*) M. T. Pope and B. W. Dale, *Q. Rev., Chem. Soc.*, 1968, **22**, 527–548; (*b*) C. M. Flynn, Jr. and G. D. Stucky, *Inorg. Chem.*, 1969, **8**, 332–334.